Advances in Atmospheric Sciences
Impact Factor: 5.8
E-alert
ISSN 0256-1530
CN 11-1925/O4

Characteristics of Energy Fluxes and Cold Frontal Effects on Energy Exchange over a Boreal Lake

Lujun XU, Huizhi LIU, Ivan MAMMARELLA, Aki VH, Joonatan ALA-KNNI, Xuefei LI, Qun DU, Yang LIU, Timo VESALA

Citation: Xu, L. J., and Coauthors 2025: Characteristics of Energy Fluxes and Cold Frontal Effects on Energy Exchange over a Boreal Lake, *Adv. Atmos. Sci.*, 42, 357–372. doi: 10.1007/s00376-024-3214-y.

View online: https://doi.org/10.1007/s00376-024-3214-y

ADVANCES IN ATMOSPHERIC SCIENCES, VOL. 42, FEBRUARY 2025, 357–372

• **Original Paper** •

Characteristics of Energy Fluxes and Cold Frontal Effects on Energy Exchange over a Boreal Lake

Lujun XU[1,2], Huizhi LIU[*3], Ivan MAMMARELLA[4], Aki VÄHÄ[4], Joonatan ALA-KÖNNI[4], Xuefei LI[4], Qun DU[1,2], Yang LIU[1,2], and Timo VESALA[*4]

[1]*State Key Laboratory of Atmospheric Boundary Layer Physics and Atmospheric Chemistry*, *Institute of Atmospheric Physics*, *Chinese Academy of Sciences*, *Beijing* 100029, *China*

[2]*University of Chinese Academy of Sciences*, *Beijing* 100864, *China*

[3]*Department of Atmospheric Sciences*, *Yunnan University*, *Kunming* 650091, *China*

[4]*Institute for Atmospheric and Earth System Research/Physics*, *Faculty of Science*, *University of Helsinki*, *Helsinki* 00014, *Finland*

(Received 29 December 2023; revised 29 May 2024; accepted 6 June 2024)

ABSTRACT

Understanding the characteristics and variations of heat exchange and evaporation of lakes is important for regional water resource management and sustainable development. Based on eddy covariance measurements over Lake Vanajavesi in southern Finland, characteristics of energy fluxes and cold frontal effects on energy exchange were investigated. The lake acted as a heat sink in spring and summer and a heat source in winter. The latent heat flux reached its minimum value in the morning and peaked in the afternoon. The diurnal variation of sensible heat flux was opposite to that of latent heat flux. Impact factors for the sensible heat flux were mainly the lake-air temperature difference and the product of lake-air temperature difference and wind speed. The latent heat flux was mainly affected by the vapor pressure deficit and the product of vapor pressure deficit and wind speed. The annual mean values of bulk transfer coefficients for momentum, heat, and water vapor were 1.98×10^{-3}, 1.62×10^{-3}, and 1.31×10^{-3}, respectively. Bulk transfer coefficients for heat and water vapor were not equal, indicating that the parameterization of energy exchange in numerical models, where the assumption that the heat coefficient equals the water vapor coefficient needs improvement. During the ice-free season, cold fronts resulted in 28 sensible heat pulses and 17 latent heat pulses, contributing to 50.59% and 34.89% of sensible and latent heat exchange in Lake Vanajavesi. These results indicate that cold fronts significantly impact the surface energy budget and evaporation over lakes.

Key words: sensible heat flux, latent heat flux, roughness length, bulk transfer coefficient, cold front

Citation: Xu, L. J., and Coauthors, 2025: Characteristics of energy fluxes and cold frontal effects on energy exchange over a boreal lake. *Adv. Atmos. Sci.*, **42**(2), 357−372, https://doi.org/10.1007/s00376-024-3214-y.

Article Highlights:

- The studied lake can regulate regional energy exchange on both daily and seasonal scales.
- Bulk transfer coefficients for heat and water vapor were not equal, indicating that the parameterization of energy exchange in numerical models, where the assumption that the heat coefficient is equal to the water vapor coefficient needs to be improved.
- Cold fronts can significantly promote sensible and latent heat exchange over lakes.

1. Introduction

There are more than 117 million lakes worldwide, covering approximately 3.7% of the Earth's non-glaciated land surface (Verpoorter et al., 2014). Lakes provide key energy, water, ecosystem, and ecological services for catchment areas (Biermann et al., 2014; Santanello et al., 2018; Wang et al., 2018) and are sensitive to global warming, acting as sentinels of climate change (Adrian et al., 2009; Woolway and Merchant, 2019). Due to global warming, lakes exhibit changes in surface water temperature, evaporation, mixing regimes, ice cover, and so on (O'Reilly et al., 2015; Rodell et al., 2018; Woolway et al., 2019). Such variations interact with one another, complicating the mechanism of the lake's physical response to climate change (Woolway et al., 2020).

* Corresponding authors: Huizhi LIU, Timo VESALA
Emails: huizhil@mail.iap.ac.cn, timo.vesala@helsinki.fi

However, the lack of long-term measurements over lakes leads to less detailed information on atmospheric energy exchanges and associated hydrological cycles (Huotari et al., 2011; Feng et al., 2016). Investigating lake–atmosphere interactive processes will improve the understanding of lake responses to global climatic variations (Huziy and Sushama, 2017; Meng et al., 2023).

Due to their large heat capacity and low surface albedo and roughness, lakes act differently from other land surfaces in the exchange of regional momentum, heat, and mass. (Xu et al., 2016; Sugita, 2020). Compared to soil and vegetated surfaces, the surface albedo of lakes is low (Xiao and Bowker, 2020; Yan et al., 2021; Du et al., 2023). The lack of reflectance leads to a large part of solar radiation being absorbed by the water surface and deeper layers (Subin et al., 2012). Due to the large heat capacity of water, the temperature of water increases more slowly than the temperature of the atmosphere (Fink et al., 2014). Further, the time lag of lake-temperature warming in spring is longer for deep water than for shallow water (Calamita et al., 2021). In late spring and summer, the lake is cooler than the atmosphere and surrounding land surfaces, thereby functioning as an energy sink (Spence et al., 2003). Beginning in late autumn and lasting through winter, the solar radiation is low; consequently, the water surface temperature becomes higher than the air temperature, allowing the lakes to transition to an energy source (Gianniou and Antonopoulos, 2007; Sun et al., 2020). This attribute of lakes brings significant thermal lag to the regional climate (Lei et al., 2021). In summer and autumn, large temperature and vapor pressure gradients between the lake surface and the overlying atmosphere favor energy flux exchanges (Zhang et al., 2023). The latent heat flux is determined by vapor pressure differences between the lake and atmosphere interface, and the sensible heat flux (H) is dependent upon the temperature difference between the water surface and the air above (Liu et al., 2012; Li et al., 2015). These turbulent fluxes are also affected by the wind speed and turbulent mixing intensity (Liu et al., 2015; Sugita et al., 2020). The evaporation of small lakes is smaller than that of large lakes, and their sensible heat flux is about twice that of large lakes (Rouse et al., 2008). Whether these physical processes of large and deep lakes, which control momentum, heat, and water exchanges between the lake and the atmosphere, apply to small and shallow lakes remains unclear (Bryan et al., 2015; Wang et al., 2019; Notaro et al., 2022).

Lake–atmosphere interactions are also influenced by large-scale synoptic processes (Gerken et al., 2013; Huang and Li, 2017; Du et al., 2018a; Arrillaga et al., 2019). Passage of large-scale synoptic processes may cause changes in temperature, wind, and humidity in the catchment area, altering the stability of the atmospheric boundary layer and the development of convection, significantly impacting the regional energy and water cycle (Gerken et al., 2014; Arrillaga et al., 2016; Yusup and Liu, 2020). The differences in the thermal and dynamic properties between lakes and land can stimulate deep convective activity and increase local precipitation (Sturman et al., 2003; Wen et al., 2015). Xu et al. (2019) found that the warm and humid flow brought by the monsoon can reduce the temperature and humidity differences between the lake and the atmosphere and suppress the exchange of matter and energy at the lake surface in Erhai Lake, southwest China.

Cold frontal activities play a significant role in regulating the exchange of surface heat fluxes and the water cycle (Liu et al., 2011; Roberts et al., 2015; Van Den Broeke, 2022). The invasion of dry and cold flow above warm and humid lake areas can increase wind speed, temperature, and humidity gradients between the lake and the atmosphere, enhancing turbulent mixing (Matias et al., 2021). In central Mississippi, cold fronts can increase the sensible and latent heat flux transport by 77% and 16%, respectively, resulting in a 167% increase in lake heat loss (Curtarelli et al., 2013). Under moderately unstable and stable conditions, the enhanced mechanical mixing promotes sensible and latent heat exchanges with increased wind speed (Yusup and Liu, 2020). Unlike the noted cooling effects when cold fronts pass by inland lakes, more than half of cold frontal passages in coastal sites present a warming effect and decreased relative humidities in the post-frontal sector (Van Den Broeke , 2022). The passage of cold fronts can also affect the local water cycle (Huang and Li, 2019; Zhang et al., 2022). As cold fronts approach, local water levels in the Wax Lake Delta, Louisiana, USA, could be elevated by even one meter (Roberts et al., 2015). These effects demonstrate the need to carefully consider the characteristics of lake–atmosphere interactions during cold frontal passage (Gallus and Segal, 1999; Curtarelli et al., 2013; Huang and Li, 2017).

The highest concentration, perimeter, and area of lakes appear at boreal and arctic latitudes (Pekel et al., 2016). High-latitude lakes are warming faster than the global average, which may have profound implications for the catchment area (Pilla et al., 2020; Noori et al., 2022). As few boreal lakes have detailed observations of long-term energy fluxes, the understanding of lake–atmosphere interactions and their response to cold fronts is limited (Spence et al., 2003; Huotari et al., 2013; Mammarella et al., 2015; Stepanenko et al., 2016). From January 2016 to January 2017, an eddy covariance measurement was conducted over Lake Vanajavesi, a boreal lake in southern Finland. Half-hourly data on temperature, wind, radiation, and energy fluxes were collected and analyzed. In this study, the main aims are (1) to provide detailed information on lake–atmosphere interactions, (2) to investigate the impact factors of turbulence fluxes, (3) to characterize variations of bulk transfer parameters, and (4) to demonstrate the significance of cold fronts in lake–atmosphere interactions. The results will benefit water resource management in lake catchment areas and assist in more accurate parameterizations of lake–atmosphere interactions in numerical weather models.

The remainder of this paper is organized as follows. Section 2 describes the data and methods used in this study. Section 3 presents and discusses the results; finally, section 4 provides a summary and conclusion.

2. Data and methods

2.1. *Site description and measurements*

Lake Vanajavesi (61°4'–61°19'N, 23°45'–24°24'E) is located in the provinces of Pirkanmaa and Kanta-Häme, southern Finland (Partanen and Hellsten, 2005; Yang et al., 2012). The average (maximum) depth of the lake is 8 m (23.89 m). Its average altitude is 79.40 m above sea level. The area of Lake Vanajavesi is about 119 km^2. The measurement site is located on the tip of a narrow peninsula along the eastern shore of the lake (Fig. 1c, 61°8'N, 24°15'E). The lake depth nearby is 5 m. A fixed platform has been established here since November 2015. Continuous measurements of meteorological variables, radiation components, and turbulent exchanges of momentum, heat, and CO_2 were conducted at this location from Jan. 2016 to Jan. 2017.

Air temperature and relative humidity were measured by a Rotronic MP102H sensor (Rotronic Instrument Corp., NY, USA) at a height of 2.5 m over the platform. The shortwave and longwave radiation components were also measured at a height of 2.5 m with a net radiometer (CNR1, Kipp & Zonen, Netherlands). All atmospheric measurements were calculated using 30-min averages for the analyses.

Turbulent exchange of momentum, heat, and mass (H_2O and CO_2) were measured by an eddy covariance (EC) system. The EC system includes an open-path CO_2/H_2O gas analyzer (LICOR, LI-7200, USA) and an ultrasonic anemometer (Metek, GmBH, Germany), also installed at a height of 2.5 m. The sample frequency of an EC system is 10 Hz. The 10-Hz raw data were processed using the EddyUH software (Mammarella et al., 2016). Spikes in the data due to instrument malfunction, weather, and physical noise were removed (Vickers and Mahrt, 1997; Foken et al., 2005). A double rotation was applied to align the x-axis into the mean horizontal wind direction and rotated the wind velocity components into a natural coordinate system (Kaimal and Finnigan, 1994). The 30-min momentum flux (τ), sensible heat flux (H), and latent heat flux (LE) were calculated using the eddy covariance method as follows:

$$\tau = -\rho u_*^2 , \tag{1}$$

$$H = \rho C_p \overline{w' T_a'} , \tag{2}$$

$$\mathrm{LE} = \lambda \rho \overline{w' q'} , \tag{3}$$

where τ is the momentum flux; H is latent heat flux; ρ is air density, $u_*$is the friction velocity; C_p is the specific heat of air at constant pressure; w is the vertical wind speed; T_a is air temperature; LE is latent heat flux; λ is latent heat of vaporization; q is the specific humidity of air. Positive fluxes are defined as upwards. Corrections for density fluctuations and frequency losses were made (Webb et al., 1980; Lee et al., 2005; Mammarella et al., 2009; Foken et al., 2012).

The footprint of the EC site was calculated using the footprint model proposed by Kljun et al. (2015) from 30-min data in 2016 (Fig. 2). The average source area responsible for contributing 90% of the flux ranges from 152 to 209 m in all directions. When the wind blows from the 110°–205° sector, the peninsula mainly affects flux exchange. Therefore, the flux data from this sector were filtered. Overall, 60.77% of H and 60.19% of LE data were selected to analyze the characteristics of lake–atmosphere interactions.

2.2. *Lake surface temperature and energy balance*

Lake surface temperature (T_s) is a key variable influencing turbulent exchange between the water surface and the atmosphere. It can be derived from the longwave radiation as follows:

$$\varepsilon \sigma T_s^4 = L_\uparrow - (1-\varepsilon) L_\downarrow \tag{4}$$

where $\varepsilon = 0.97$ is surface emissivity; $\sigma = 5.67 \times 10^{-8}$ W m^{-2} K^{-4} is the Stefan-Bolzmann constant; $L_\uparrow$ is upward

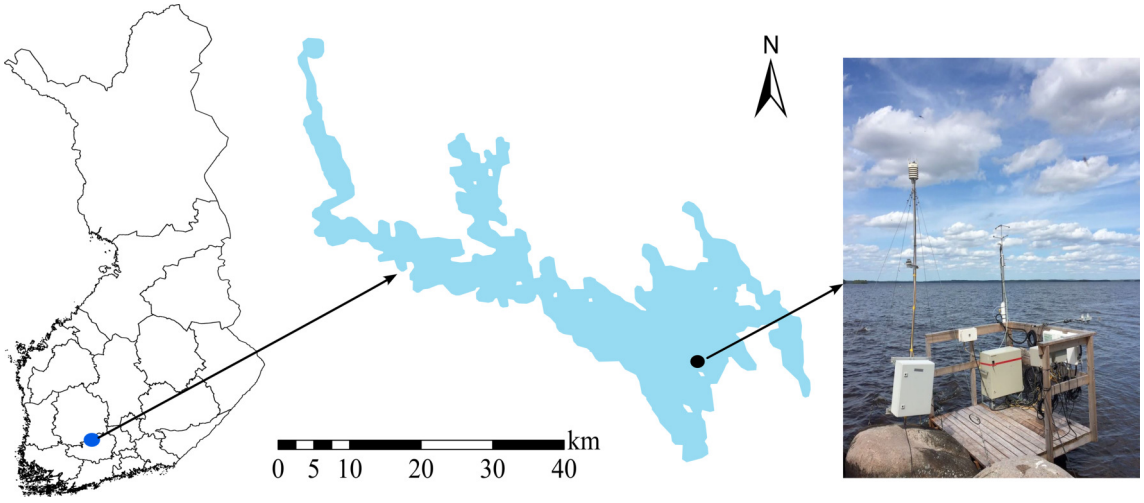

Fig. 1. The measurement platform above Lake Vanajavesi. The blue (black) point represents the location of Lake Vanajavesi (the measurement site).

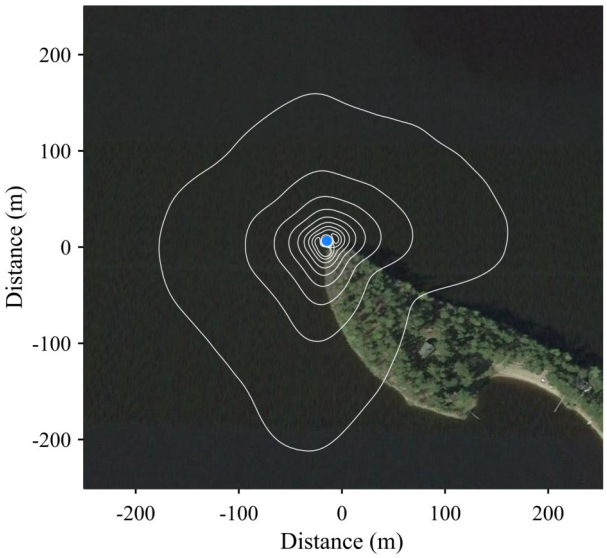

Fig. 2. Footprint climatology for the EC site. The white contours represent the percentage of the accumulated flux footprint from 10%–90% in increments of 10%. The blue dot indicates the location of the EC tower. The satellite photograph was taken from Google Earth.

longwave radiation; $L_{\downarrow}$ is downward longwave radiation.

Lake surface energy balance is usually defined as (Nordbo et al., 2011):

$$R_n - \Delta Q = H + \mathrm{LE} + \Delta Q_B + \Delta Q_F + \Delta Q_P \,, \tag{5}$$

where R_n is the net radiation; ΔQ is the change of heat storage in the lake per unit area; H is the sensible heat flux; LE is the latent heat flux; ΔQ_B is the heat flux into the bottom sediments; ΔQ_F is the net heat flux from lake runoff and outlet; ΔQ_P is the heat flux due to precipitation. The signs of H and LE are positive upwards, ΔQ is positive when the lake gains heat and the rest are positive downwards. The last three terms are small and can be neglected. Then Eq. (2) can be simplified as:

$$R_n - \Delta Q \approx H + \mathrm{LE} \,, \tag{6}$$

where $R_n - \Delta Q$ is the available energy. Units of all fluxes are W m^{-2}. The change in heat storage of the lake per unit area (ΔQ) can be calculated from Eq. (3) as:

$$\Delta Q = R_n - H + \mathrm{LE} \,. \tag{7}$$

2.3. *Surface roughness and bulk transfer coefficients*

The surface roughness length and bulk transfer coefficients were calculated in this study to characterize the lake–atmosphere exchange. According to Monin-Obukhov similarity theory, the wind profile in the surface layer can be written as (Stull, 1988):

$$\frac{\kappa U}{u_*} = \ln\frac{z-d}{z_{0m}} - \psi_m(\zeta) \,, \tag{8}$$

where $\kappa = 0.4$ is the von Kármán constant; U is the wind speed; u_* is the friction velocity; z is measurement height, d is displacement height (can be set to zero for lake surface); z_{0m} is the aerodynamic roughness length; $\psi_m(\zeta)$ is the stability function of wind profile; $\zeta = z/L$ is the stability parameter. L is the Obukhov length, which is defined as follows:

$$L = \frac{-\rho u_*^3 (T_a + 273.16)(1 + 0.61q)}{kg\left[\dfrac{H}{C_p} + 0.61\dfrac{(T_a + 273.16)\mathrm{LE}}{\lambda}\right]} \,. \tag{9}$$

The aerodynamic roughness length z_{0m} can be derived from Eq. (8) as:

$$z_{0m} = z\exp\left[-\frac{\kappa U}{u_*} - \psi_m(\zeta)\right] \,, \tag{10}$$

$$\begin{cases} \psi_m = 2\ln\left(\dfrac{1+x}{2}\right) + \ln\left(\dfrac{1+x^2}{2}\right) - 2\arctan\left(x + \dfrac{\pi}{2}\right) & \zeta < 0 \\ \psi_m = -5\zeta & \zeta > 0 \end{cases} \,, \tag{11}$$

$$x = (1 - 16\zeta)^{\frac{1}{4}} \,. \tag{12}$$

The thermodynamic roughness length z_{0h} can be derived through the following formulae (Dyer, 1974; Verhoef et al., 1997):

$$\ln\frac{z_{0m}}{z_{0h}} = \frac{\kappa u_* (T_s - T_a)}{H/\rho C_p} - \left[\ln\frac{z-d}{z_{0m}} - \psi_h(\zeta)\right] \,, \tag{13}$$

$$\begin{cases} \psi_h(\zeta) = 2\ln\left(\dfrac{1+x^2}{2}\right) & \zeta < 0 \\ \psi_h(\zeta) = -5\zeta & \zeta > 0 \end{cases} \,, \tag{14}$$

where T_s is lake surface temperature; T_a is air temperature at height z; H is sensible heat flux; ρ is air density; C_p is the specific heat of air at constant pressure; $\psi_h(\zeta)$ is the stability function of the temperature profile.

In the surface layer, the bulk transfer coefficients for momentum, heat, and water vapor can be derived as (Andreas, 1987):

$$\begin{cases} C_d = \dfrac{\tau}{\rho U^2} \\ C_h = \dfrac{H}{\rho c_p U(T_s - T_a)} \\ C_q = \dfrac{\mathrm{LE}}{\rho\lambda U(q_s - q)} \end{cases} \,, \tag{15}$$

where C_d, C_h, and C_q are the bulk transfer coefficients for momentum, heat, and water vapor, respectively; λ is the latent heat of vaporization; q_s is the specific humidity of the lake surface; q is the specific humidity at height z.

3. Results and discussion

3.1. *Meteorological conditions*

The meteorological conditions at Vanajavesi Lake in 2016 are shown in Fig. 3. The annual air temperature was 6.52°C in 2016. The monthly average air temperature was below zero in winter and early spring. January was the coldest month, with an average air temperature of –3.03°C. July was the warmest month, with an average air temperature of 17.88°C. The average daily temperature range was highest in December (25.07°C) and lowest in August (12.3°C). The average lake surface temperature during the ice-free season (April–October) was 11.74°C. It was highest in July; the same was found for Lake Lappajärvi, also located in southern Finland (Rontu et al., 2019). The lake surface temperature was lower than the air temperature in April and May, while in October, it was higher.

The prevailing wind throughout the year was southwesterly (Fig. 3b). The average wind speed was 3.06 m s^{-1}. On the seasonal scale, the daily wind speed in winter was larger than in other seasons. The average wind speeds in spring, summer, autumn, and winter were 3.13, 2.11, 3.18, and 3.80 m s^{-1}, respectively. The daily wind speed reached its maximum in December (8.37 m s^{-1}) and minimum in May (0.66 m s^{-1}).

3.2. *Radiation*

Characteristics of radiation transfer at Lake Vanajavesi from March 2016 through January 2017 are shown in Fig. 4 (radiation data in Jan. 2016 and Feb. 2016 was missing). On a daily scale, the solar radiation reached its peak (about 600 W m^{-2} in May) at 1300 LST (LST= UTC+8 hours), which was similar to that of mid-latitude lakes (Wang et al., 2014). From the perspective of the seasonal scale, the solar radiation in summer was higher than in other seasons, peaking in May and reaching its minimum in December. The outgoing shortwave radiation in winter and early spring was much higher than during any other time of the year. In March, the

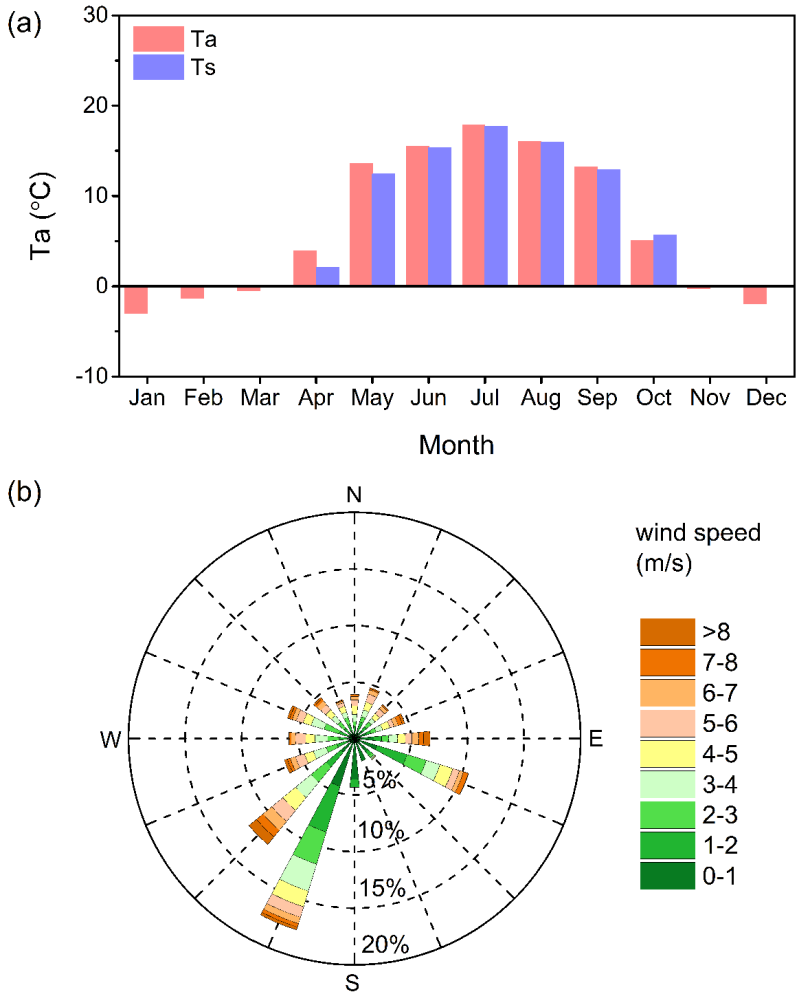

Fig. 3. (a) Monthly averaged air temperature and lake surface temperature. (b) The wind rose observed at Lake Vanajavesi.

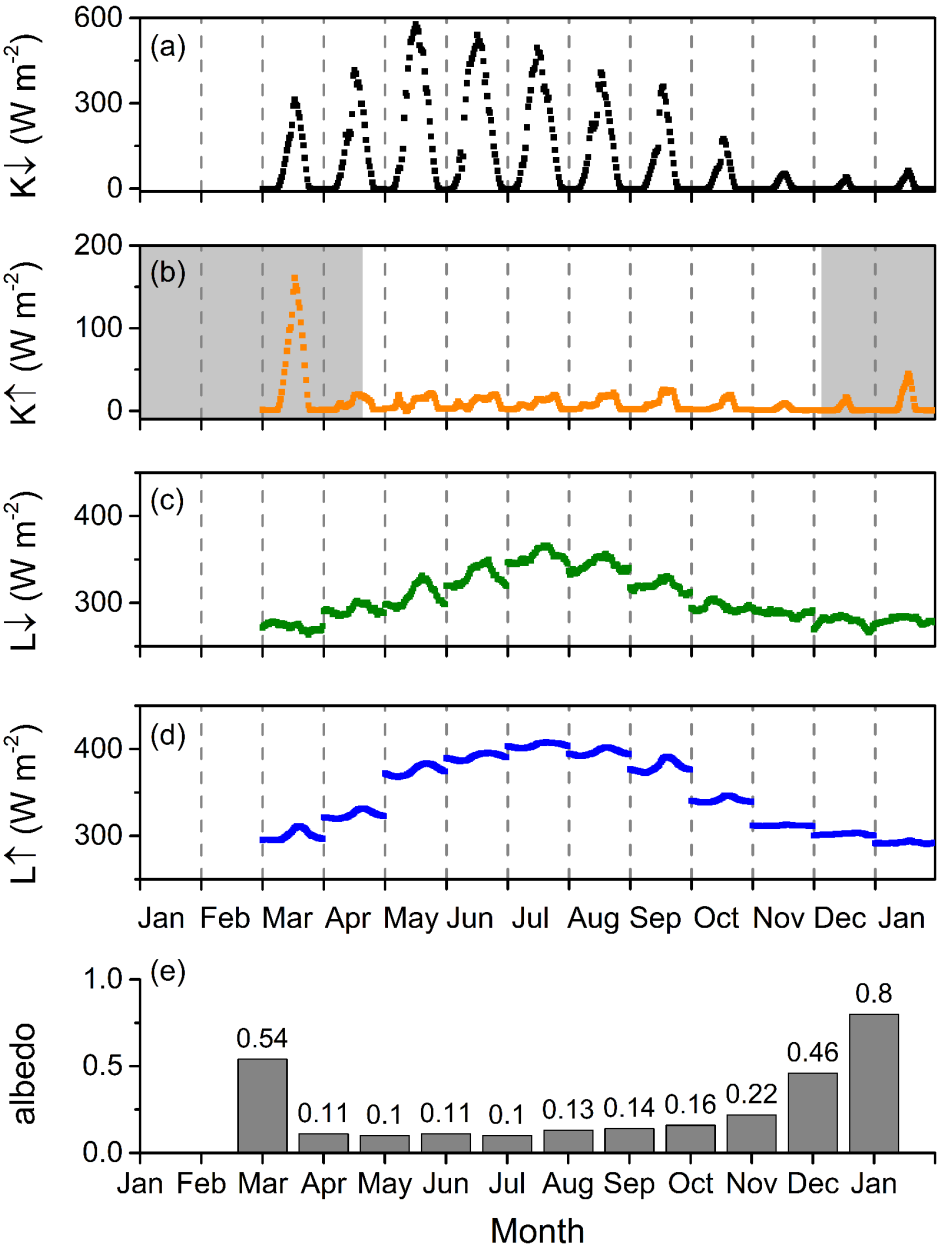

Fig. 4. (a) Monthly averaged diurnal cycle of downward shortwave radiation; (b) monthly averaged diurnal cycle of upward shortwave radiation, the shaded area indicates ice cover period; (c) monthly averaged diurnal cycle of downward longwave radiation; (d) monthly averaged diurnal cycle of upward longwave radiation; (e) monthly averaged albedo.

outgoing shortwave radiation could reach 167 W m^{-2} at local noon; however, in other months, it was less than 60 W m^{-2}. The variation of outgoing shortwave radiation was mainly affected by surface albedo. The solar elevation angle, ice cover, and attributes of the water controlled the seasonal variations of surface albedo (Li et al., 2021; Du et al., 2023). In winter and early spring, ice and snow covered the lake. During that period, the surface albedo was much higher than in summer when the lake surface is liquid water. It follows that the surface albedo peaked in January (0.8) and was at a minimum in July (0.1). In summer, it increased after sunrise, reaching a certain level rapidly (less than 50 W m^{-2}) and lasted until sunset.

The incoming longwave radiation ranged from 263 to 366 W m^{-2} (Fig. 4c). It was largely affected by atmospheric moisture and the amount and height of clouds (de Kok et al., 2020). The outgoing longwave radiation ranged from 294 to 408 W m^{-2} (Fig. 4d) and was positively correlated to the surface water temperature. On the daily timescale, both incoming and outgoing longwave radiation peaked in the

afternoon (nearly 1500 LST) and obtained their lowest value in the early morning (about 0600 LST). The longwave radiation was higher in summer than that in other seasons. Both incoming and outgoing longwave radiation were highest in July and lowest in January.

3.3. *Energy exchange*

The monthly averaged diurnal cycle of energy exchanges is shown in Fig. 5. The net radiation was calculated from the four components of radiation shown in Fig. 4. The change of stored heat flux in the lake was calculated from Eq. (4). The net radiation and change in lake-storage heat flux data were missing in January and February in 2016. The net radiation ranged from –81 W m^{-2} to 505 W m^{-2}. On a seasonal timescale, the net radiation peaked in May and transitioned to mainly negative values in December. On the daily timescale, the net radiation peaked at noon (1300-1400 LST). The daily variation amplitude was largest in May. The pattern of the change in lake-storage heat flux was similar to that of net radiation. It ranged from –241 W m^{-2} to 452 W m^{-2}. The diurnal variation was higher than that at Lake Valkea-Kotinen, also in southern Finland. This may be a consequence of Lake Vanajavesi being deeper and larger, which leads to higher wind speeds and stronger mechanically induced mixing (Nordbo et al., 2011).

The sensible heat flux (H) ranged from –27 W m^{-2} to 56 W m^{-2}. It was mainly negative in winter, indicating that the lake released heat to the atmosphere. On the daily timescale, the sensible heat flux reached its maximum in the early morning and was lowest in the afternoon from April to October. The diurnal variation of the sensible heat flux was small during the ice-covered period when the temperature gradient between the lake and the atmosphere was small. During

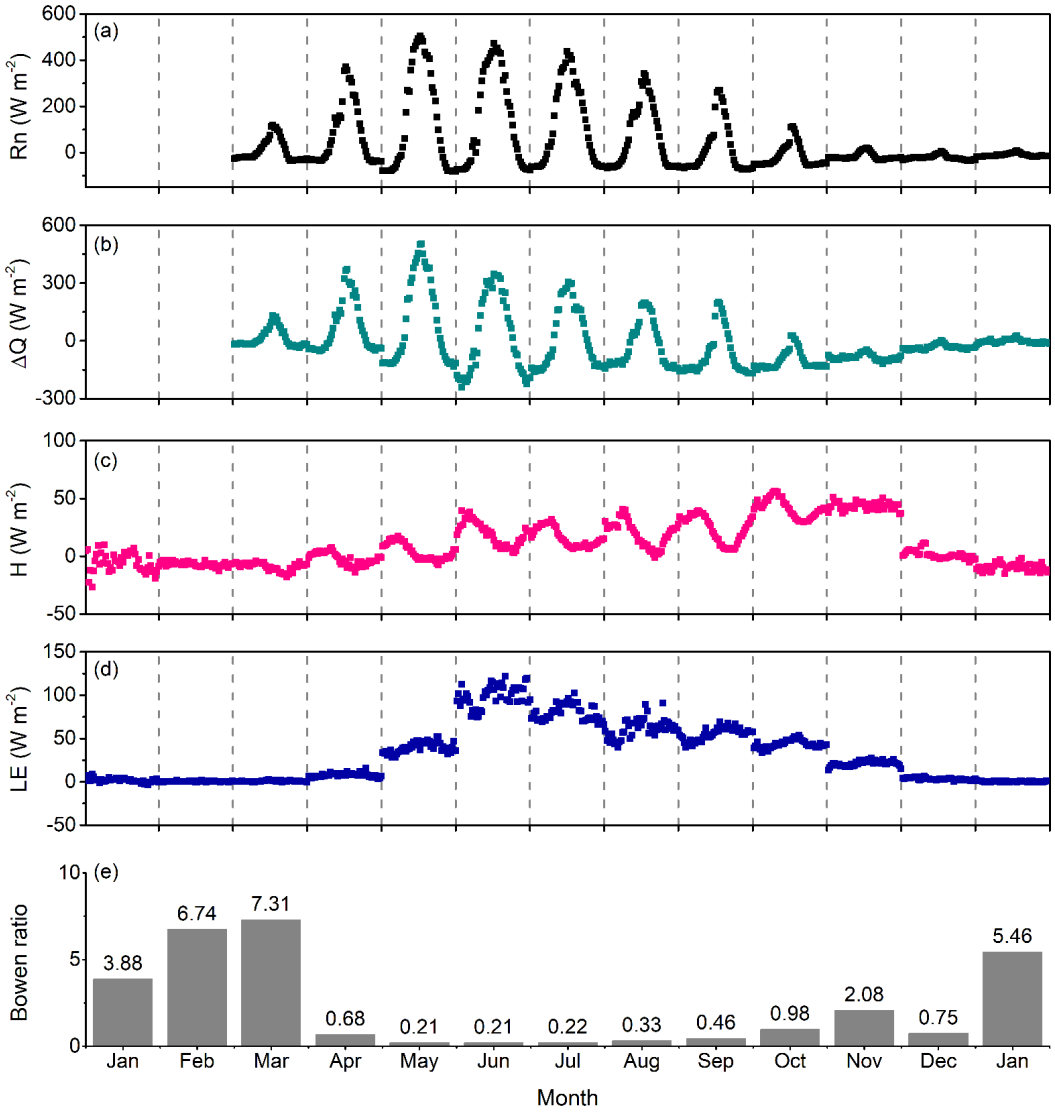

Fig. 5. (a) The monthly averaged diurnal cycle of net radiation; (b) monthly averaged diurnal cycle of the change in lake storage heat flux; (c) monthly averaged diurnal cycle of sensible heat flux; (d) monthly averaged diurnal cycle of latent heat flux; (e) monthly averaged Bowen ratio.

that time, the Bowen ratio (sensible heat flux divided by latent heat flux) was greater than 1, indicating that the available energy was primarily due to the sensible heat flux. While during the ice-free season, the latent heat flux dominated. In summer, the Bowen ratio was smaller than 0.4. It was similar to the Bowen ratio of the Ross Barnett Reservoir in Mississippi, suggesting that most of the available energy released from the lake was consumed by evaporation rather than through heating the atmosphere by sensible heat flux (Liu et al., 2009).

The latent heat flux (LE) was nearly zero during ice-covered periods and increased after the ice began to melt. The latent heat flux reached its maximum in June when the vapor pressure deficit was high. The latent heat flux showed obvious diurnal variation during the ice-free season. The diurnal variation of latent heat flux was opposite to that of sensible heat flux, reaching its minimum value in the morning and peaking in the afternoon. In the evening, the latent heat flux was still positive, indicating nocturnal evaporation of the water surface, which lies in contrast with the other land surfaces, where the latent heat flux was often negligibly small during the night (Xiang et al., 2017).

The seasonal variation of energy fluxes is shown in Fig. 6 (the net radiation and change in lake storage heat flux data were missing in January–February, 2016). The monthly average net radiation was positive from March–September and negative in other months. It was highest in June (143.47 W m^{-2}) and lowest in December (–21.95 W m^{-2}). The monthly averaged latent heat flux also peaked in June (99.01 W m^{-2}) and declined after that. The seasonal variation of monthly average sensible heat flux was opposite to that of latent heat flux. It was 19.37 W m^{-2} in June and increased after that. The monthly average sensible heat flux was at its maximum in November (43.45 W m^{-2}). During the ice-covered season, the monthly average sensible heat flux was negative, indicating that the lake released heat to the atmosphere. The monthly averaged lake storage heat flux was positive from March–July and negative in other months. It peaked in May (94.13 W m^{-2}) and was at a minimum in October (–102.63 W m^{-2}).

The lake tended to regulate its regional energy exchange on the seasonal timescale (Fig. 6b). After the ice

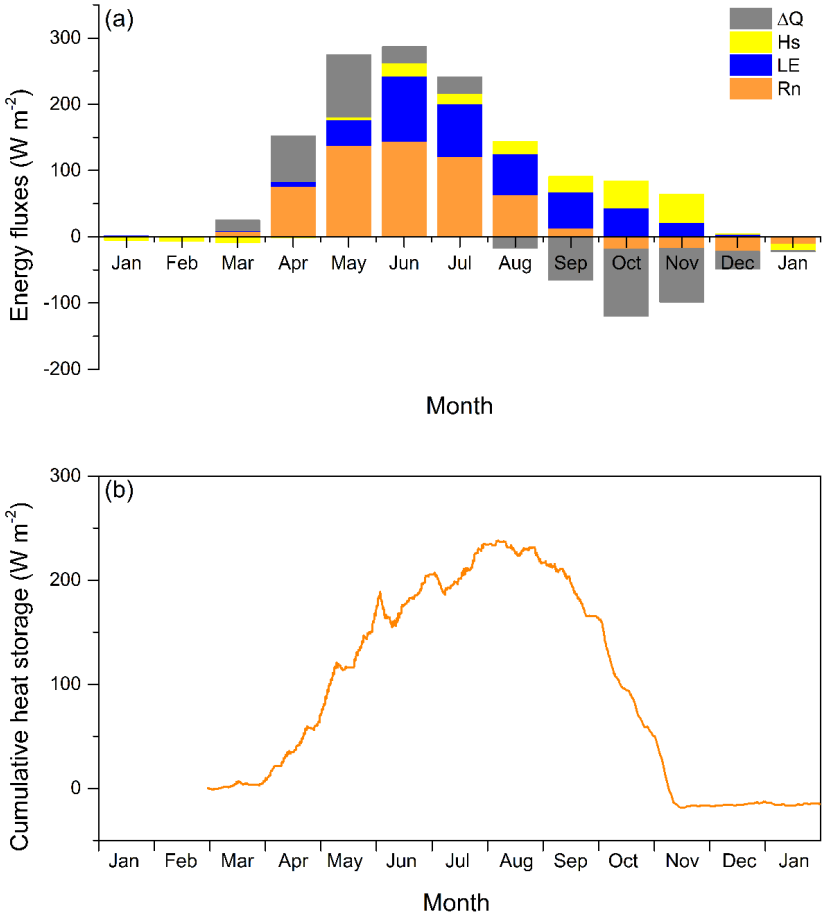

Fig. 6. (a) The seasonal variation of energy fluxes and (b) cumulative heat storage change of the lake.

began to melt, the lake started to accumulate heat in its water, acting as a heat sink. The accumulated heat flux reached its maximum on August 14 (233.58 MJ m^{-2}), a value similar to Lake Valkea-Kotinen (232 MJ m^{-2}), also located in southern Finland (Nordbo et al., 2011). After that, the lake began to release heat. The release period (74 days) was shorter than the accumulation period (118 days). This was partly due to the lake overturning in November when it rapidly released the heat stored in deep water to the atmosphere.

Factors affecting sensible and latent heat flux on different timescales are shown in Fig. 7. All available timesteps were used to calculate correlations for the whole day. For the calculation of correlations during the daytime, only timesteps whose downward shortwave radiation was positive were used. The other timesteps were used for the calculation of nighttime factors. The sensible heat flux was mainly governed by the lake-air temperature difference ($T_s - T_a$), and the product of lake-air temperature difference and wind speed [$U(T_s - T_a)$]. Their correlation coefficients ranged from 0.78 to 0.95 and increased with longer timescales. The latent heat flux was mainly controlled by vapor pressure deficit ($ew - ea$), and the product of vapor pressure deficit and wind speed [$U(ew - ea)$]. Wind speed had a positive effect on both the sensible and latent heat fluxes. The close relationship between $U(T_s - T_a)$ and H, and $U(ew - ea)$and LE were also observed in other lakes (Du et al., 2018b). Relative humidity negatively affected latent heat flux, especially on a monthly timescale.

Driving factors for sensible and latent heat flux during daytime and nighttime were mostly the same, but there were still some differences. On a monthly timescale, net radiation had a positive effect on heat flux during the daytime, while at night, it transitioned to a negative effect. Increases in daytime net radiation promoted stronger sensible and latent heat exchanges. While at night, the net radiation attained a negative value. The smaller the value, the stronger the energy exchange. It is noted that in some other studies, net radiation played a minor role in surface energy fluxes on daily and monthly scales, indicating that observation data over more lakes is needed to adequately describe the details of the energy exchange (Lenters et al., 2005; Liu et al., 2009).

Energy exchange across the lake-atmosphere interface is also affected by other factors (Gao et al., 2018; Zhao and Liu, 2018; Zeng and Zhang, 2020; Pierre et al., 2022). Meng et al. (2020) found that the stratification of the atmospheric surface layer played an important role in regulating the turbulent fluxes. Under stable conditions, the sensible heat flux was found to be closely related to wind speed and the lake-air temperature difference, while under unstable conditions, they showed no obvious relationship. The total cloud cover (sunshine duration) had a positive (negative) effect on energy exchange on daily and monthly timescales (Du et al., 2018a). Weather conditions also affected the energy exchange between the lake and the atmosphere. The maximum (minimum) heat fluxes usually followed the passage of low (high) pressure in northern Lake Huron (Laird et al., 2002). On different timescales, however, $U(T_s - T_a)$ and $U(ew - ea)$were the most common and critical factors in determining sensible and latent heat fluxes.

3.4. *Surface roughness lengths and bulk transfer coefficients*

The aerodynamic and aerothermodynamic roughness lengths (z_{0m} and z_{0h}) and bulk transfer coefficients (C_d, C_h, and C_q) were calculated when there was no precipitation (parameters for calculating C_h and C_q were missing in some months). The annual mean values of z_{0m} and z_{0h} were 3.25 × 10^{-2} m and 4.59 × 10^{-3} m, respectively. The ratio between z_{0m} and z_{0h} was 7.08. z_{0m} was large in winter and spring, possibly a consequence of the strong winds and high waves common to that period (Fig. 8). Seasonal variation of z_{0h} was different from z_{0m}. It was high in summer and autumn and low in winter.

The annual mean values of the bulk transfer coeffi-

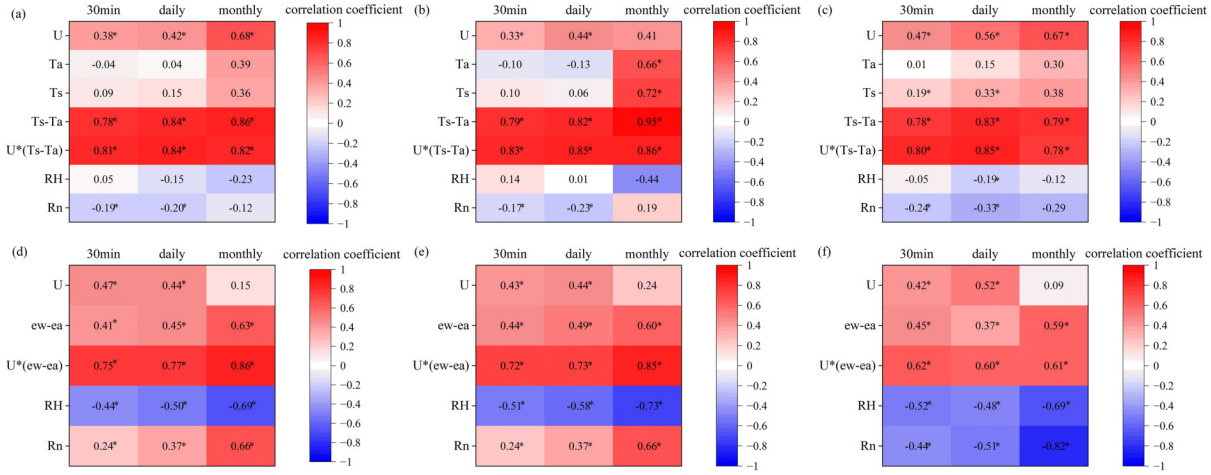

Fig. 7. Impact factors of sensible heat flux for (a) the whole day; (b) daytime; (c) nighttime. The impact factors of latent heat flux during (d) the whole day; (e) daytime; (f) nighttime. Asterisks (*) represent statistical significance at $p \leq 0.05$.

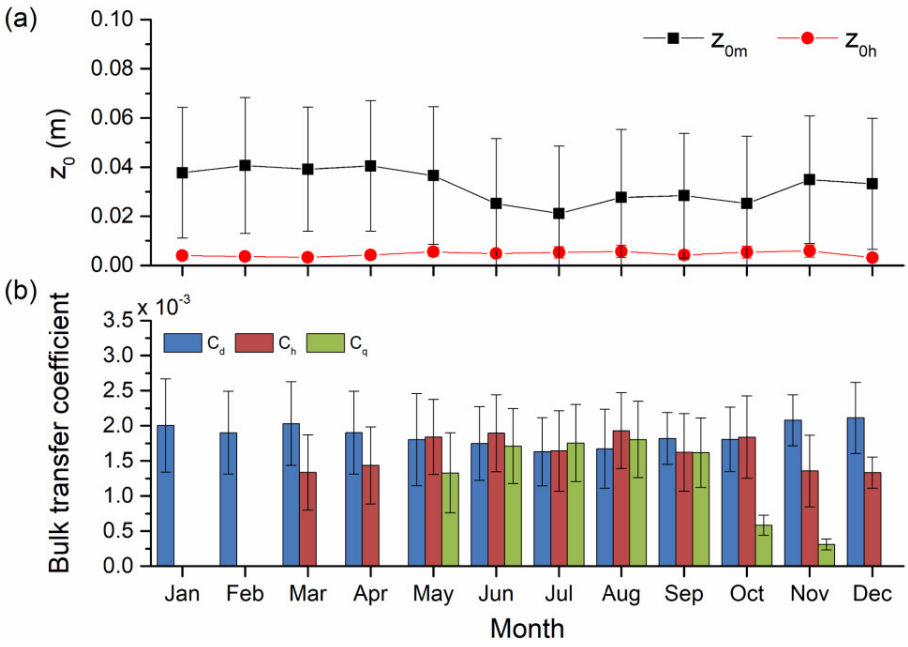

Fig. 8. (a) Monthly averaged aerodynamic roughness length; (b) monthly averaged bulk transfer coefficients (The bars indicate the standard deviation).

cients, C_d, C_h, and C_q, were 1.98×10^{-3}, 1.62×10^{-3}, and 1.31×10^{-3}, respectively. C_d was similar to the drag coefficients calculated by the eddy-covariance technique using data from more than 30 reservoirs and lakes of different depths and sizes (Guseva et al., 2023). C_d was largest in winter and summer, while C_h and C_q were large in summer. When the atmospheric stratification was unstable (most of the time over the lake), the bulk transfer coefficients decreased as the wind speed increased. The ratio between C_d and C_h was 1.22, and C_q/C_h was 0.81. This differs from what some numerical and empirical models assume (Stepanenko et al., 2014). For example, the WRF and CLM4.5 employ a constant value for the drag coefficient and assume $C_q = C_h$ (Subin et al., 2012; Oleson et al., 2013). This approach results in biased estimations of lake temperature and evaporation and leads to errors in weather and climate prediction models, indicating that the parameterization of roughness lengths in numerical models needs to be improved (Drews, 2013; Woolway et al., 2015; Chen et al., 2020; Sun et al., 2020).

Surface roughness lengths and bulk transfer coefficients can vary with the size and depth of the lake. Due to a larger size and wind-induced waves, the bulk transfer coefficient for momentum of Lake Vanajavesi (1.98×10^{-3}) was larger than that of a small lake (1.40×10^{-3}) in the Nam-Co Basin, southwest China (Wang et al., 2019). The roughness length and standard bulk transfer coefficient for momentum were 80% and 21% higher, respectively, for a large lake than for a small lake, while the roughness lengths and standard bulk transfer coefficient for heat and water are one order of magnitude and 7% lower, respectively (Wang et al., 2019). Compared with deep water, the surface temperature in a shallow lake was more sensitive to the roughness lengths (Li et al., 2018). These results indicate that lake area and depth should be considered in the parameterization of surface roughness lengths and bulk transfer coefficients.

3.5. *Effects of cold fronts on energy exchange*

The influence of variable cold frontal activities on the surface energy fluxes was investigated during the ice-free season. The ice-free season was considered to begin on the day when the surface albedo was permanently reduced to less than a tenth, $\alpha < 0.1$, and ends on the day when $\alpha > 0.5$ (Ala-Könni et al., 2022). In 2016, the ice-free season lasted for 231 days. It began on April 18 and ended on December 5.

According to Arrillaga et al. (2018), cold front days were identified as days whose equivalent potential temperature variation in 6 h was lower than 1.45 K at 700 hPa. The variation of equivalent potential temperature (θ_e) was calculated as follows:

$$\frac{\Delta\theta_e}{\Delta t} = \frac{\Delta\theta}{\Delta t} + \frac{l_v}{C_{pd}}\frac{\Delta r}{\Delta t}, \tag{16}$$

where θ is the potential temperature; r is the water vapor mixing ratio, $l_v = 2.46 \times 10^6$ J kg^{-1} is the latent heat of vaporization; C_{pd}=1005 J kg^{-1} K^{-1} is the specific heat of dry air at constant pressure. The θ and r data at 700 hPa were sourced from ECMWF ERA5 data (https://www.ecmwf.int/en/forecasts/dataset/ecmwf-reanalysis-v5).

The passage of cold fronts was usually accompanied by decreased air temperature and increased wind speed, which resulted in pulses of sensible and latent heat flux. A sensible (or latent) heat flux pulse was identified as days when the daily average sensible (or latent) heat flux was larger than 1.5 times the 10-day running mean (Liu et al., 2011). When a sensible (or latent) heat flux pulse occurred within the pas-

sage of cold fronts, it was determined to be an effect of cold fronts on surface energy exchange. Within the cold frontal days of 2016, a total of 28 sensible heat flux pluses (*H* pulses) and 17 latent heat flux pulses (LE pulses) were found, covering 43 and 31 days (18.61% and 13.42% of the ice-free season).

A typical *H* and LE pulse is presented in Fig. 9. On 8 June 2016, a cold front passed over the observation site in Vanajavesi Lake. The cold front arrived at 0200 LST on June 8 and lasted about 59 hours. It led to a dramatic increase in wind speed and a rapid decrease in air temperature. When the cold front passed the observation site, the wind speed increased by approximately 8.28 m s^{-1}, and the wind direction changed from southerly to northwesterly. Meanwhile, the air temperature dropped by 9.94°C, and the water temperature decreased by 5.49°C. The air vapor pressure decreased from 10.7 hPa to 4.1 hPa. As the surface vapor pressure is well documented to equate to the saturation vapor pressure at the lake-atmosphere interface, the vapor pressure deficit between the lake and the atmosphere became larger (Ambaum, 2020; Zhao et al., 2022). The wind speed and temperature difference (vapor pressure deficit) were the main factors that affected the sensible (latent) heat flux. As a result, the sensible heat flux (*H*) increased from –25.48 W m^{-2} to 151 W m^{-2}, and the latent heat flux increased from 29.46 W m^{-2} to 398.86 W m^{-2} in Lake Vanajavesi. The sensible and latent heat flux pulse in Lake Vanajavesi was similar to the heat flux exchange in a reservoir in Central Brazil. As a cold front passed the reservoir, the sensible heat flux increased to a value five times larger than the initial energy flux (Curtarelli et al., 2013). During the entire ice-free season, the *H* (LE) pulses contributed about 49.44% (34.89%) to the total *H* (LE), indicating that cold fronts significantly affect the surface energy exchange.

The changes in air mass properties caused by the passage of cold fronts affected lake–atmosphere exchange processes and significantly enhanced the surface energy fluxes. This phenomenon has also been confirmed by eddy covariance observations in other lakes. Based on eddy covariance observations in the Ross Barnett Reservoir (in Mississippi), Liu et al. (2009) found that during the passage of a cold front, the latent and sensible heat fluxes increased by 7.3 and 2.7

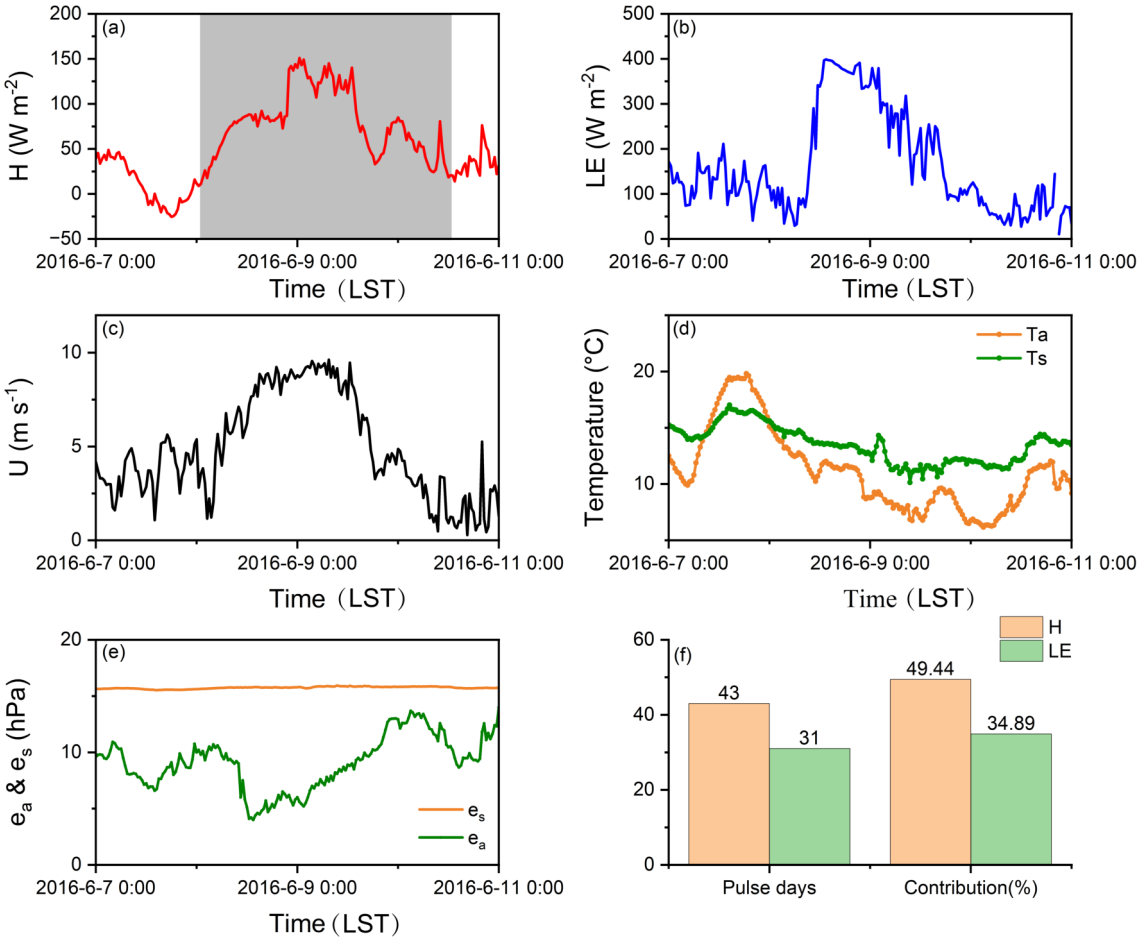

Fig. 9. Time-series data of the 30-min mean (a) sensible heat flux, (b) latent heat flux, (c) wind speed, (d) air temperature and water surface temperature, (e) vapor pressure for the water-air interface and the overlying air, and (f) days and contribution of *H* and LE pulses. The data represent a typical *H* and LE pulse as a result of a high-wind event behind a cold front that passed over the site on 8 June 2016. The shaded area in (a) indicates the duration of the cold front.

times, respectively. Compared to deep lakes, shallow lakes respond faster to the passage of cold fronts (Liu et al., 2019). In Taihu Lake, located in Jiangsu Province, eastern China, cold frontal days only accounted for 16.4% of the cold season but contributed 34.9% and 51.7% of the latent and sensible heat fluxes for the total cold season, respectively (Liu et al., 2019). There is currently little research on quantifying the impact of cold frontal activities on lake–atmosphere interactions. Exploring the responses of lake surface energy fluxes to cold frontal events can provide a scientific basis for predicting the impacts of extreme cold events on lakes in the future.

4. Conclusions

Based on observational data from Lake Vanajavesi in 2016, characteristics of energy fluxes and cold frontal effects on energy exchange were investigated. The annual air temperature and wind speed were 6.52°C and 3.06 m s^{-1} in 2016. The air temperature was highest in July and lowest in January. The seasonal variation of wind speed was opposite to air temperature. It peaked in December and had its minimum value in May. The surface albedo was also high in winter and low in late spring and summer. In winter and early spring, when the lake surface was covered by ice and snow, the monthly average albedo exceeded 0.5. During that period, the upward shortwave radiation reached its maximum value of 167 W m^{-2} at noon. The seasonal variation of surface albedo was mainly controlled by the solar elevation angle, ice cover, and the attributes of the water.

The energy fluxes show obvious diurnal and seasonal variations. The energy fluxes were high in late spring and summer and low in winter when the lake was ice-covered. The net radiation and the change in heat storage of the lake per unit area peaked at noon and was low at night. The sensible heat flux had its maximum value in the morning and minimum value in the afternoon. In contrast, the diurnal variation of latent heat flux demonstrated the opposite pattern. The lake acted as a heat sink in spring and summer and a heat source in autumn and winter. The available energy in the daytime was mainly dominated by latent heat flux during the ice-free season, while during the ice-covered season, the sensible heat flux was dominant. The sensible heat flux was mainly affected by the lake-air temperature difference and the product of the lake-air temperature difference and the wind speed, whereas the latent heat flux was controlled by vapor pressure deficit and the product of vapor pressure deficit and wind speed.

Characteristics of surface roughness lengths and bulk transfer coefficients were also analyzed. The annual mean values of aerodynamic and aerothermodynamic roughness lengths (z_{0m} and z_{0h}) were 3.25×10^{-2} m and 4.59×10^{-3} m. The value of aerothermodynamic roughness length was approximately one-seventh of the aerodynamic roughness length. Owning to the presence of strong winds and high waves, the aerodynamic roughness length had a larger value in winter and spring. The annual mean value of bulk transfer coefficients (C_d, C_h, and C_q) were 1.98×10^{-3}, 1.62×10^{-3}, and 1.31×10^{-3}, respectively. Under unstable conditions, the bulk transfer coefficients decreased as wind speed increased.

Cold fronts significantly impact the surface energy budget and evaporation over water. Along with cold-frontal passage, there appeared to be a rapid increase in wind speed and a decrease in temperature. Due to its large heat capacity, the cooling rate of the lake was slower than that of the atmosphere. Consequently, the lake-atmosphere temperature difference and vapor pressure deficit became larger, leading to sensible and latent heat pulses, respectively. Cold fronts contributed 49.44% and 34.89% of sensible and latent heat exchange during the ice-free season.

These results demonstrate features of energy fluxes and cold-frontal effects on energy exchange at a boreal lake. The consequences may vary depending on lake location, coverage area, water depth, mixing regime, and eutrophication status. Future research, including strengthening long-term observations of lake variables from space and developing advanced parameterization of lake-atmosphere interaction processes, will improve our understanding of lake responses and their associated feedback to climate change.

Acknowledgements This study was supported by funds from the National Natural Science Foundation of China (Grant Nos: 42275079, 41975017, 42411530052, and 42161144010) and the Second Tibetan Plateau Scientific Expedition and Research (STEP) program (Grant No. 2019QZKK0105).

Funding note: Open Access funding provided by University of Helsinki (including Helsinki University Central Hospital)

REFERENCES

Adrian, R., and Coauthors, 2009: Lakes as sentinels of climate change. *Limnology and Oceanography*, **54**(6part2), 2283–2297, https://doi.org/10.4319/lo.2009.54.6_part_2.2283.

Ala-Könni, J., K. M. Kohonen, M. Leppäranta, and I. Mammarella, 2022: Validation of turbulent heat transfer models against eddy covariance flux measurements over a seasonally ice-covered lake. *Geoscientific Model Development*, **15**(12), 4739–4755, https://doi.org/10.5194/gmd-15-4739-2022.

Ambaum, M. H. P., 2020: Accurate, simple equation for saturated vapour pressure over water and ice. *Quart. J. Roy. Meteor. Soc.*, **146**(733), 4252–4258, https://doi.org/10.1002/qj.3899.

Andreas, E. L., 1987: A theory for the scalar roughness and the scalar transfer coefficients over snow and sea ice. *Bound.-Layer Meteorol.*, **38**(1–2), 159–184, https://doi.org/10.1007/BF00121562.

Arrillaga, J. A., C. Yagüe, M. Sastre, and C. Román-Cascón, 2016: A characterisation of sea-breeze events in the eastern Cantabrian coast (Spain) from observational data and WRF simulations. *Atmospheric Research*, **181**, 265–280, https://doi.org/10.1016/j.atmosres.2016.06.021.

Arrillaga, J. A., J. V.-G. de Arellano, F. Bosveld, H. K. Baltink, C. Yagüe, M. Sastre, and C. Román-Cascón, 2018: Impacts of afternoon and evening sea-breeze fronts on local turbulence, and on CO_2 and radon-222 transport. *Quart. J. Roy. Meteor. Soc.*, **144**(713), 990–1011, https://doi.org/10.1002/qj.3252.

Arrillaga, J. A., C. Yagüe, C. Román-Cascón, M. Sastre, M. A. Jiménez, G. Maqueda, and J. V.-G. de Arellano, 2019: From weak to intense downslope winds: Origin, interaction with boundary-layer turbulence and impact on CO_2 variability. *Atmospheric Chemistry and Physics*, **19**(7), 4615–4635, https://doi.org/10.5194/acp-19-4615-2019.

Biermann, T., W. Babel, W. Q. Ma, X. L. Chen, E. Thiem, Y. M. Ma, and T. Foken, 2014: Turbulent flux observations and modelling over a shallow lake and a wet grassland in the Nam Co basin, Tibetan Plateau. *Theor. Appl. Climatol.*, **116**(1–2), 301–316, https://doi.org/10.1007/s00704-013-0953-6.

Bryan, A. M., A. L. Steiner, and D. J. Posselt, 2015: Regional modeling of surface-atmosphere interactions and their impact on Great Lakes hydroclimate. *J. Geophys. Res.: Atmos.*, **120**(3), 1044–1064, https://doi.org/10.1002/2014JD022316.

Calamita, E., S. Piccolroaz, B. Majone, and M. Toffolon, 2021: On the role of local depth and latitude on surface warming heterogeneity in the Laurentian Great Lakes. *Inland Waters*, **11**(2), 208–222, https://doi.org/10.1080/20442041.2021.1873698.

Chen, F., C. Zhang, M. T. Brett, and J. M. Nielsen, 2020: The importance of the wind-drag coefficient parameterization for hydrodynamic modeling of a large shallow lake. *Ecological Informatics*, **59**, 101106, https://doi.org/10.1016/j.ecoinf.2020.101106.

Curtarelli, M., E. Alcântara, C. Rennó, and J. Stech, 2013: Effects of cold fronts on MODIS-derived sensible and latent heat fluxes in Itumbiara reservoir (Central Brazil). *Advances in Space Research*, **52**(9), 1668–1677, https://doi.org/10.1016/j.asr.2013.07.037.

de Kok, R. J., J. F. Steiner, M. Litt, P. Wagnon, I. Koch, M. F. Azam, and W. W. Immerzeel, 2020: Measurements, models and drivers of incoming longwave radiation in the Himalaya. *International Journal of Climatology*, **40**(2), 942–956, https://doi.org/10.1002/joc.6249.

Drews, C., 2013: Using wind setdown and storm surge on Lake Erie to calibrate the air-sea drag coefficient. *PLoS ONE*, **8**(8), e72510, https://doi.org/10.1371/journal.pone.0072510.

Du, J., P.-A. Jacinthe, K. S. Song, and H. Zhou, 2023: Water surface albedo and its driving factors on the turbid lakes of Northeast China. *Ecological Indicators*, **146**, 109905, https://doi.org/10.1016/j.ecolind.2023.109905.

Du, Q., H. Z. Liu, L. J. Xu, Y. Liu, and L. Wang, 2018a: The monsoon effect on energy and carbon exchange processes over a highland lake in the southwest of China. *Atmospheric Chemistry and Physics*, **18**(20), 15 087–15 104, https://doi.org/10.5194/acp-18-15087-2018.

Du, Q., H. Z. Liu, Y. Liu, L. Wang, L. J. Xu, J. H. Sun, and A. L. Xu, 2018b: Factors controlling evaporation and the CO_2 flux over an open water lake in southwest of China on multiple temporal scales. *International Journal of Climatology*, **38**(13), 4723–4739, https://doi.org/10.1002/joc.5692.

Dyer, A. J., 1974: A review of flux-profile relationships. *Bound.-Layer Meteorol.*, **7**(3), 363–372, https://doi.org/10.1007/BF00240838.

Feng, J. W., H. Z. Liu, J. H. Sun, and L. Wang, 2016: The surface energy budget and interannual variation of the annual total evaporation over a highland lake in Southwest China. *Theor. Appl. Climatol.*, **126**(1–2), 303–312, https://doi.org/10.1007/s00704-015-1585-9.

Fink, G., M. Schmid, and A. Wüest, 2014: Large lakes as sources and sinks of anthropogenic heat: Capacities and limits. *Water Resour. Res.*, **50**(9), 7285–7301, https://doi.org/10.1002/2014WR015509.

Foken, T., M. Göockede, M. Mauder, L. Mahrt, B. Amiro, and W. Munger, 2005: Post-field data quality control. *Handbook of Micrometeorology: A Guide for Surface Flux Measurement and Analysis*, X. Lee et al., Eds., Springer, 181–208, https://doi.org/10.1007/1-4020-2265-4_9.

Foken, T., R. Leuning, S. P. Oncley, M. Mauder, and M. Aubinet, 2012. In: Aubinet, M., Vesala, T., Papale, D. (Eds.), Eddy Covariance: A Practical Guide to Measurement and Data Analysis. Springer, Dordrecht, 85–132.

Gallus, W. A., and M. Segal, 1999: Cold front acceleration over Lake Michigan. *Wea. Forecasting*, **14**(5), 771–781, https://doi.org/10.1175/1520-0434(1999)014<0771:CFAOLM>2.0.CO;2.

Gao, Z. M., H. P. Liu, D. Li, G. G. Katul, and P. D. Blanken, 2018: Enhanced temperature-humidity similarity caused by entrainment processes with increased wind shear. *J. Geophys. Res.: Atmos.*, **123**, 4110–4121, https://doi.org/10.1029/2017JD028195.

Gerken, T., W. Babel, F. L. Sun, M. Herzog, Y. M. Ma, T. Foken, and H.-F. Graf, 2013: Uncertainty in atmospheric profiles and its impact on modeled convection development at Nam Co Lake, Tibetan Plateau. *J. Geophys. Res.: Atmos.*, **118**(22), 12 317–12 331, https://doi.org/10.1002/2013JD020647.

Gerken, T., T. Biermann, W. Babel, M. Herzog, Y. M. Ma, T. Foken, and H.-F. Graf, 2014: A modelling investigation into lake-breeze development and convection triggering in the Nam Co Lake basin, Tibetan Plateau. *Theor. Appl. Climatol.*, **117**(1–2), 149–167, https://doi.org/10.1007/s00704-013-0987-9.

Gianniou, S. K., and V. Z. Antonopoulos, 2007: Evaporation and energy budget in Lake Vegoritis, Greece. *J. Hydrol.*, **345**(3–4), 212–223, https://doi.org/10.1016/j.jhydrol.2007.08.007.

Guseva, S., and Coauthors, 2023: Bulk transfer coefficients estimated from eddy-covariance measurements over lakes and reservoirs. *J. Geophys. Res.: Atmos.*, **128**(2), e2022JD037219, https://doi.org/10.1029/2022JD037219.

Huang, W., and C. Y. Li, 2017: Cold front driven flows through multiple inlets of Lake Pontchartrain Estuary. *J. Geophys. Res.: Oceans*, **122**(11), 8627–8645, https://doi.org/10.1002/2017JC012977.

Huang, W., and C. Y. Li, 2019: Spatial variation of cold front wind-driven circulation and quasi-steady state balance in Lake Pontchartrain Estuary. *Estuarine, Coastal and Shelf Science*, **224**, 154–170, https://doi.org/10.1016/j.ecss.2019.04.031.

Huotari, J., S. Haapanala, J. Pumpanen, T. Vesala, and A. Ojala, 2013: Efficient gas exchange between a boreal river and the atmosphere. *Geophys. Res. Lett.*, **40**(21), 5683–5686, https://doi.org/10.1002/2013GL057705.

Huotari, J., and Coauthors, 2011: Long-term direct CO_2 flux measurements over a boreal lake: Five years of eddy covariance data. *Geophys. Res. Lett.*, **38**(18), L18401, https://doi.org/10.1029/2011GL048753.

Huziy, O., and L. Sushama, 2017: Lake–river and lake–atmosphere interactions in a changing climate over Northeast Canada. *Climate Dyn.*, **48**(9–10), 3227–3246, https://doi.org/10.1007/s00382-016-3260-y.

Kaimal, J. C., and J. J. Finnigan, 1994: *Atmospheric Boundary Layer Flows: Their Structure and Measurement*. Oxford University Press, https://doi.org/10.1093/oso/9780195062397.001.0001.

Kljun, N., P. Calanca, M. W. Rotach, and H. P. Schmid, 2015: A simple two-dimensional parameterisation for Flux Footprint Prediction (FFP). *Geoscientific Model Development*, **8**(11), 3695–3713, https://doi.org/10.5194/gmd-8-3695-2015.

Laird, N. F., and D. A. R. Kristovich, 2002: Variations of sensible and latent heat fluxes from a great lakes buoy and associated synoptic weather patterns. *Journal of Hydrometeorology*, **3**, 3–12, https://doi.org/10.1175/1525-7541(2002)003<0003:VOSALH>2.0.CO;2.

Lee, X., W. Massman, and B. Law, 2005: *Handbook of Micrometeorology: A Guide for Surface Flux Measurement and Analysis*. Springer, https://doi.org/10.1007/1-4020-2265-4.

Lei, Y. B., T. D. Yao, K. Yang, Lazhu, Y. M. Ma, and B. W. Bird, 2021: Contrasting hydrological and thermal intensities determine seasonal lake-level variations – a case study at Paiku Co on the southern Tibetan Plateau. *Hydrology and Earth System Sciences*, **25**(6), 3163–3177, https://doi.org/10.5194/hess-25-3163-2021.

Lenters, J. D., T. K. Kratz, and C. J. Bowser, 2005: Effects of climate variability on lake evaporation: Results from a long-term energy budget study of Sparkling Lake, northern Wisconsin (USA). *J. Hydrol.*, **308**(1–4), 168–195, https://doi.org/10.1016/j.jhydrol.2004.10.028.

Li, Z. G., S. Lyu, Y. H. Ao, L. J. Wen, L. Zhao, and S. Y. Wang, 2015: Long-term energy flux and radiation balance observations over Lake Ngoring, Tibetan Plateau. *Atmospheric Research*, **155**, 13–25, https://doi.org/10.1016/j.atmosres.2014.11.019.

Li, Z. G., S. Lyu, L. L. Wen, L. Zhao, X. H. Meng, and Y. H. Ao, 2018: Effect of roughness lengths on surface energy and the planetary boundary layer height over high-altitude Ngoring Lake. *Theor Appl Climatol*, **133**, 1191–1205, https://doi.org/10.1007/s00704-017-2258-7.

Li, Z. J., and Coauthors, 2021: Diurnal cycle model of lake ice surface albedo: A case study of Wuliangsuhai Lake. *Remote Sensing*, **13**(16), 3334, https://doi.org/10.3390/rs13163334.

Liu, H. P., Q. Y. Zhang, and G. Dowler, 2012: Environmental controls on the surface energy budget over a large southern inland water in the United States: An analysis of one-year eddy covariance flux data. *Journal of Hydrometeorology*, **13**(6), 1893–1910, https://doi.org/10.1175/JHM-D-12-020.1.

Liu, H. P., P. D. Blanken, T. Weidinger, A. Nordbo, and T. Vesala, 2011: Variability in cold front activities modulating cool-season evaporation from a southern inland water in the USA. *Environmental Research Letters*, **6**, 024022, https://doi.org/10.1088/1748-9326/6/2/024022.

Liu, H. P., Y. Zhang, S. H. Liu, H. M. Jiang, L. Sheng, and Q. L. Williams, 2009: Eddy covariance measurements of surface energy budget and evaporation in a cool season over southern open water in Mississippi. *J. Geophys. Res.: Atmos.*, **114**(D4), D04110, https://doi.org/10.1029/2008JD010891.

Liu, H. Z., J. W. Feng, J. H. Sun, L. Wang, and A. L. Xu, 2015: Eddy covariance measurements of water vapor and CO_2 fluxes above the Erhai Lake. *Science China Earth Sciences*, **58**(3), 317–328, https://doi.org/10.1007/s11430-014-4828-1.

Liu, Q., W. Wang, W. Xiao, S. J. Jing, M. Zhang, Y. B. Hu, Z. Zhang, and Y. H. Xie, 2019: Quantifying the effects of different cold air events on latent and sensible heat fluxes of Lake Taihu. *Journal of Lake Sciences*, **31**(4), 1144–1156, https://doi.org/10.18307/2019.0425. (in Chinese with English abstract)

Mammarella, I., O. Peltola, A. Nordbo, L. Järvi, and Ü. Rannik, 2016: Quantifying the uncertainty of eddy covariance fluxes due to the use of different software packages and combinations of processing steps in two contrasting ecosystems. *Atmospheric Measurement Techniques*, **9**(10), 4915–4933, https://doi.org/10.5194/amt-9-4915-2016.

Mammarella, I., S. Launiainen, T. Gronholm, P. Keronen, J. Pumpanen, Ü. Rannik, and T. Vesala, 2009: Relative humidity effect on the high-frequency attenuation of water vapor flux measured by a closed-path eddy covariance system. *J. Atmos. Oceanic Technol.*, **26**(9), 1856–1866, https://doi.org/10.1175/2009JTECHA1179.1.

Mammarella, I., and Coauthors, 2015: Carbon dioxide and energy fluxes over a small boreal lake in Southern Finland. *J. Geophys. Res.: Biogeosci.*, **120**(7), 1296–1314, https://doi.org/10.1002/2014JG002873.

Matias de Faria, D., L. de Souza Cardoso, and D. Motta Marques, 2021: Cold fronts induce changes in phycoperiphyton structure in a shallow lake: Wind forces drive algae succession and nutrient availability. *Limnologica*, **91**, 125926, https://doi.org/10.1016/j.limno.2021.125926.

Meng, X. H., and Coauthors, 2023: Dataset of comparative observations for land surface processes over the semi-arid alpine grassland against alpine lakes in the source region of the Yellow River. *Adv. Atmos. Sci.*, **40**(6), 1142–1157, https://doi.org/10.1007/s00376-022-2118-y.

Meng, X. N., H. Z. Liu, Q. Du, Y. Liu, and L. J. Xu, 2020: Factors controlling the latent and sensible heat fluxes over Erhai Lake under different atmospheric surface layer stability conditions. *Atmospheric and Oceanic Science Letters*, **13**(5), 400–406, https://doi.org/10.1080/16742834.2020.1769450.

Noori, R., S. M. Bateni, M. Saari, M. Almazroui, and A. T. Haghighi, 2022: Strong warming rates in the surface and bottom layers of a boreal lake: Results from approximately six decades of measurements (1964–2020). *Earth and Space Science*, **9**(2), e2021EA001973, https://doi.org/10.1029/2021EA001973.

Nordbo, A., S. Launiainen, I. Mammarella, M. Leppäranta, J. Huotari, A. Ojala, and T. Vesala, 2011: Long-term energy flux measurements and energy balance over a small boreal lake using eddy covariance technique. *J. Geophys. Res.: Atmos.*,

116(D2), D02119, https://doi.org/10.1029/2010JD014542.

Notaro, M., J. Jorns, and L. Briley, 2022: Representation of lake–atmosphere interactions and lake-effect snowfall in the laurentian great lakes basin among HighResMIP global climate models. *J. Atmos. Sci.*, **79**(5), 1325–1347, https://doi.org/10.1175/JAS-D-21-0249.1.

Oleson, K. W., and Coauthors, 2013: Technical description of version 4.5 of the Community Land Model (CLM). No. NCAR/TN-503+STR, https://doi.org/10.5065/D6RR1W7M.

O'Reilly, C. M., and Coauthors, 2015: Rapid and highly variable warming of lake surface waters around the globe. *Geophys. Res. Lett.*, **42**(24), 10 773–10 781, https://doi.org/10.1002/2015GL066235.

Partanen, S., and S. Hellsten, 2005: Changes of emergent aquatic macrophyte cover in seven large boreal lakes in Finland with special reference to water level regulation. *Fennia*, **183**, 57–79.

Pekel, J.-F., A. Cottam, N. Gorelick, and A. S. Belward, 2016: High-resolution mapping of global surface water and its long-term changes. *Nature*, **540**(7633), 418–422, https://doi.org/10.1038/nature20584.

Pierre, A., P. E. Isabelle, D. F. Nadeau, A. Thiboult, A. Perelet, A. N. Rousseau, F. Anctil, and A. Deschamps, 2022: Estimating sensible and latent heat fluxes over an inland water body using optical and microwave scintillometers. *Bound.-Layer Meteorol.*, **185**, 277–308, https://doi.org/10.1007/s10546-022-00732-7.

Pilla, R. M., and Coauthors, 2020: Deeper waters are changing less consistently than surface waters in a global analysis of 102 lakes. *Scientific Reports*, **10**(1), 20514, https://doi.org/10.1038/s41598-020-76873-x.

Roberts, H. H., R. D. DeLaune, J. R. White, C. Y. Li, C. E. Sasser, D. Braud, E. Weeks, and S. Khalil, 2015: Floods and cold front passages: Impacts on coastal marshes in a river diversion setting (Wax Lake Delta Area, Louisiana). *Journal of Coastal Research*, **315**(5), 1057–1068, https://doi.org/10.2112/JCOASTRES-D-14-00173.1.

Rodell, M., J. S. Famiglietti, D. N. Wiese, J. T. Reager, H. K. Beaudoing, F. W. Landerer, and M. H. Lo, 2018: Emerging trends in global freshwater availability. *Nature*, **557**(7707), 651–659, https://doi.org/10.1038/s41586-018-0123-1.

Rontu, L., K. Eerola, and M. Horttanainen, 2019: Validation of lake surface state in the HIRLAM v.7.4 numerical weather prediction model against in situ measurements in Finland. *Geoscientific Model Development*, **12**(8), 3707–3723, https://doi.org/10.5194/gmd-12-3707-2019.

Rouse, W. R., P. D. Blanken, N. Bussières, A. E. Walker, C. J. Oswald, W. M. Schertzer, and C. Spence, 2008: An investigation of the thermal and energy balance regimes of great slave and great bear lakes. *Journal of Hydrometeorology*, **9**(6), 1318–1333, https://doi.org/10.1175/2008JHM977.1.

Santanello, J. A., and Coauthors, 2018: Land–atmosphere interactions: The LoCo perspective. *Bull. Amer. Meteor. Soc.*, **99**(6), 1253–1272, https://doi.org/10.1175/BAMS-D-17-0001.1.

Spence, C., W. R. Rouse, D. Worth, and C. Oswald, 2003: Energy budget processes of a small northern lake. *Journal of Hydrometeorology*, **4**(4), 694–701, https://doi.org/10.1175/1525-7541(2003)004<0694:EBPOAS>2.0.CO;2.

Stepanenko, V., I. Mammarella, A. Ojala, H. Miettinen, V. Lykosov, and T. Vesala, 2016: LAKE 2.0: A model for temperature, methane, carbon dioxide and oxygen dynamics in lakes. *Geoscientific Model Development*, **9**(5), 1977–2006, https://doi.org/10.5194/gmd-9-1977-2016.

Stepanenko, V., K. D. Jöhnk, E. Machulskaya, M. Perroud, Z. Subin, A. Nordbo, I. Mammarella, and D. Mironov, 2014: Simulation of surface energy fluxes and stratification of a small boreal lake by a set of one-dimensional models. *Tellus A: Dynamic Meteorology and Oceanography*, **66**, 21389, https://doi.org/10.3402/tellusa.v66.21389.

Stull, R. B., 1988: *An Introduction to Boundary Layer Meteorology*. Springer, https://doi.org/10.1007/978-94-009-3027-8.

Sturman, A. P., and Coauthors, 2003: The Lake Tekapo Experiment (LTEX): An investigation of atmospheric boundary layer processes in complex terrain. *Bull. Amer. Meteor. Soc.*, **84**(3), 371–380, https://doi.org/10.1175/BAMS-84-3-371.

Subin, Z. M., W. J. Riley, and D. Mironov, 2012: An improved lake model for climate simulations: Model structure, evaluation, and sensitivity analyses in CESM1. *Journal of Advances in Modeling Earth Systems*, **4**(1), M02001, https://doi.org/10.1029/2011MS000072.

Sugita, M., 2020: Spatial variability of the surface energy balance of Lake Kasumigaura and implications for flux measurements. *Hydrological Sciences Journal*, **65**(3), 401–414, https://doi.org/10.1080/02626667.2019.1701676.

Sugita, M., S. Ogawa, and M. Kawade, 2020: Wind as a main driver of spatial variability of surface energy balance over a shallow 10^2-km^2 scale lake: Lake Kasumigaura, Japan. *Water Resour. Res.*, **56**(8), e2020WR027173, https://doi.org/10.1029/2020WR027173.

Sun, X.-Z. L., Liang, T. J. Ling, M. Xu, and X. Lee, 2020: Improving a multilevel turbulence closure model for a shallow lake in comparison with other 1-D models. *Journal of Advances in Modeling Earth Systems*, **12**(7), e2019MS001971, https://doi.org/10.1029/2019MS001971.

Van Den Broeke, M., 2022: Seasonally and diurnally varying cold front effects along the minnesotan north shore of lake superior. *Atmosphere*, **13**(3), 441, https://doi.org/10.3390/atmos13030441.

Verhoef, A., H. A. R. De Bruin, and B. J. J. M. Van Den Hurk, 1997: Some practical notes on the parameter kB−1 for sparse vegetation. *J. Appl. Meteorol.*, **36**(5), 560–572, https://doi.org/10.1175/1520-0450(1997)036<0560:SPNOTP>2.0.CO;2.

Verpoorter, C., T. Kutser, D. A. Seekell, and L. J. Tranvik, 2014: A global inventory of lakes based on high-resolution satellite imagery. *Geophys. Res. Lett.*, **41**(18), 6396–6402, https://doi.org/10.1002/2014GL060641.

Vickers, D., and L. Mahrt, 1997: Quality control and flux sampling problems for tower and aircraft data. *J. Atmos. Oceanic Technol.*, **14**(3), 512–526, https://doi.org/10.1175/1520-0426(1997)014<0512:QCAFSP>2.0.CO;2.

Wang, B. B., Y. M. Ma, Y. Wang, Z. B. Su, and W. Q. Ma, 2019: Significant differences exist in lake-atmosphere interactions and the evaporation rates of high-elevation small and large lakes. *J. Hydrol.*, **573**, 220–234, https://doi.org/10.1016/j.jhydrol.2019.03.066.

Wang, W., X. Lee, W. Xiao, S. D. Liu, N. Schultz, Y. W. Wang, M. Zhang, and L. Zhao, 2018: Global lake evaporation accelerated by changes in surface energy allocation in a warmer climate. *Nature Geoscience*, **11**(6), 410–414, https://doi.org/10.1038/s41561-018-0114-8.

Wang, W., and Coauthors, 2014: Temporal and spatial variations in radiation and energy balance across a large freshwater

lake in China. *J. Hydrol.*, **511**, 811–824, https://doi.org/10.1016/j.jhydrol.2014.02.012.

Webb, E. K., G. I. Pearman, and R. Leuning, 1980: Correction of flux measurements for density effects due to heat and water vapour transfer. *Quart. J. Roy. Meteor. Soc.*, **106**(447), 85–100, https://doi.org/10.1002/qj.49710644707.

Wen, L. J., S. H. Lv, Z. G. Li, L. Zhao, and N. Nagabhatla, 2015: Impacts of the two biggest lakes on local temperature and precipitation in the Yellow River source region of the Tibetan Plateau. *Advances in Meteorology*, **2015**, 248031, https://doi.org/10.1155/2015/248031.

Woolway, R. I., and C. J. Merchant, 2019: Worldwide alteration of lake mixing regimes in response to climate change. *Nature Geoscience*, **12**(4), 271–276, https://doi.org/10.1038/s41561-019-0322-x.

Woolway, R. I., B. M. Kraemer, J. D. Lenters, C. J. Merchant, C. M. O'Reilly, and S. Sharma, 2020: Global lake responses to climate change. *Nature Reviews Earth & Environment*, **1**(8), 388–403, https://doi.org/10.1038/s43017-020-0067-5.

Woolway, R. I., I. D. Jones, D. P. Hamilton, S. C. Maberly, K. Muraoka, J. S. Read, R. L. Smyth, and L. A. Winslow, 2015: Automated calculation of surface energy fluxes with high-frequency lake buoy data. *Environmental Modelling and Software*, **70**, 191–198, https://doi.org/10.1016/j.envsoft.2015.04.013.

Woolway, R. I., C. J. Merchant, J. Van Den Hoek, C. Azorin-Molina, P. Nõges, A. Laas, E. B. Mackay, and I. D. Jones, 2019: Northern Hemisphere atmospheric stilling accelerates lake thermal responses to a warming world. *Geophys. Res. Lett.*, **46**(21), 11 983–11 992, https://doi.org/10.1029/2019GL082752.

Xiang, T. T., E. R. Vivoni, D. J. Gochis, and G. Mascaro, 2017: On the diurnal cycle of surface energy fluxes in the North American monsoon region using the WRF-Hydro modeling system. *J. Geophys. Res.: Atmos.*, **122**, 9024–9049, https://doi.org/10.1002/2017JD026472.

Xiao, B., and M. A. Bowker, 2020: Moss-biocrusts strongly decrease soil surface albedo, altering land-surface energy balance in a dryland ecosystem. *Science of the Total Environment*, **741**, 140425, https://doi.org/10.1016/j.scitotenv.2020.140425.

Xu, L. J., H. Z. Liu, Q. Du, and L. Wang, 2016: Evaluation of the WRF-lake model over a highland freshwater lake in southwest China. *J. Geophys. Res.: Atmos.*, **121**(23), 13 989–14 005, https://doi.org/10.1002/2016JD025396.

Xu, L. J., H. Z. Liu, Q. Du, L. Wang, L. Yang, and J. H. Sun, 2019: Differences of atmospheric boundary layer characteristics between pre-monsoon and monsoon period over the Erhai Lake. *Theor. Appl. Climatol.*, **135**(1–2), 305–321, https://doi.org/10.1007/s00704-018-2386-8.

Yan, H., S. Q. Wang, J. H. Dai, J. B. Wang, J. Chen, and H. H. Shugart, 2021: Forest greening increases land surface albedo during the main growing period between 2002 and 2019 in China. *J. Geophys. Res.: Atmos.*, **126**(6), e2020JD033582, https://doi.org/10.1029/2020JD033582.

Yang, Y., M. Leppäranta, B. Cheng, and Z. J. Li, 2012: Numerical modelling of snow and ice thicknesses in Lake Vanajavesi, Finland. *Tellus A: Dynamic Meteorology and Oceanography*, **64**, 17202, https://doi.org/10.3402/tellusa.v64i0.17202.

Yusup, Y., and H. P. Liu, 2020: Effects of persistent wind speeds on turbulent fluxes in the water-atmosphere interface. *Theor. Appl. Climatol.*, **140**(1–2), 313–325, https://doi.org/10.1007/s00704-019-03084-4.

Zeng, J., and Q. Zhang, 2020: The trends in land surface heat fluxes over global monsoon domains and their responses to monsoon and precipitation. *Scientific Reports*, **10**, 5762, https://doi.org/10.1038/s41598-020-62467-0.

Zhang, Q., C. Y. Li, W. Huang, J. Lin, M. Hiatt, and V. H. Rivera-Monroy, 2022: Water circulation driven by cold fronts in the Wax Lake Delta (Louisiana, USA). *Journal of Marine Science and Engineering*, **10**(3), 415, https://doi.org/10.3390/jmse10030415.

Zhang, Y., C.-B. An, L.-Y. Zheng, L.-Y. Liu, W.-S. Zhang, C. Lu, and Y.-Z. Zhang, 2023: Assessment of lake area in response to climate change at varying elevations: A case study of Mt. Tianshan, Central Asia. *Science of the Total Environment*, **869**, 161665, https://doi.org/10.1016/J.SCITOTENV.2023.161665.

Zhao, G., Y. Li, L. M. Zhou, and H. L. Gao, 2022: Evaporative water loss of 1.42 million global lakes. *Nature Communications*, **13**(1), 3686, https://doi.org/10.1038/S41467-022-31125-6.

Zhao, X. S., and Y. B. Liu, 2018: Variability of surface heat fluxes and its driving forces at different time scales over a large ephemeral lake in China. *J. Geophys. Res.: Atmos.*, **123**, 4939–4957, https://doi.org/10.1029/2017JD027437.